FISSION FRAGMENTS BINARY BRAKE-UP AT CROSSING OF THE SOLID-STATE FOILS

A.O. Strekalovsky[1], D.V. Kamanin[1], Yu.V. Pyatkov[2,1], Z.I. Goryainova[1], V.E. Zhuchko[1], A.A. Alexandrov[1], I.A. Alexandrova[1], R. Korsten[3], V. Malaza[3], E.A. Kuznetsova[1], O.V. Strekalovsky[4,1]

[1]Joint Institute for Nuclear Research, Dubna, Russia
[2]National Nuclear Research University MEPhI (Moscow Engineering Physics Institute), Moscow, Russia
[3]University of Stellenbosch, Faculty of Military Science, Military Academy, Saldanha 7395, South Africa
[4]Dubna State University, 141980 Dubna, Russia

INTRODUCTION

Earlier we discussed [1–3] the manifestations of a new original effect appeared at the crossing of metal foils by fission fragments (FF). A significant mass deficit in the total mass M_{sum} of the fission fragments detected in coincidence with ions knocked out from the foil was observed. It has been shown that at large angles of scattering of the knocked-out ions, predominantly conventional elastic Rutherford scattering occurs at energies below the Coulomb barrier. As the result, M_{sum} corresponds to the mean mass of the mother system after emission of fission neutrons (no missing mass). In contrast, in near frontal impacts, the fission fragment misses essential part of its mass; and the bulk of the brake-up residuals show the magic nucleon compositions. Here we present one of the new results, obtained using thick carbon foil as a degrader.

EXPERIMENT

The experiment was performed at the LIS (Light Ions Spectrometer) spectrometer in FLNR (JINR). The layout of the setup is shown in figure 1. LIS setup in the current modification is a double-armed time-of-flight spectrometer, which includes five micro-channels plates based time detectors (1–5), and two PIN diodes (6, 7). Compared to the previous version of the spectrometer [1–3], all time-of-flights were measured using only micro-channel plates based time detectors, in order to exclude an influence of the plasma delay effect in the PIN diode. Each PIN diode provides information for estimation of both FF energy and time-of-flight. Solid foils (degraders) of different thicknesses can be placed in the detector (2). The aperture for fission fragments, detected in coincidence in the opposite PIN diodes, does not exceed 3°.

The data acquisition system consists of the fast digitizer CAEN DT5742 and a personal computer. The digital images of all the signals were obtained for further off-line processing. Mass reconstruction procedure used is presented in Ref. [4]. The construction of the spectrometer allows measuring of the FF mass M_{tt} using two velocities calculated via time-of-flights at the bases (*a* and *c*). Thus, the fragment's mass M_{1tt} before the fragment passes the degrader (9) in the arm-1 of the spectrometer was reconstructed. The mass M_{1te} of the same fragment after passing the degrader was calculated using "velocity-energy" method, which involves measuring the FF time-of-flight at the base (*b)* and the FF energy using PIN diode (6). Thus, we know the mass of each FF before and after it crosses the degrader-foil for their

comparison event-by-event. The reference arm-2 is free from the degrader and serves to demonstrate a conventional FF mass spectrum obtained in the same experiment.

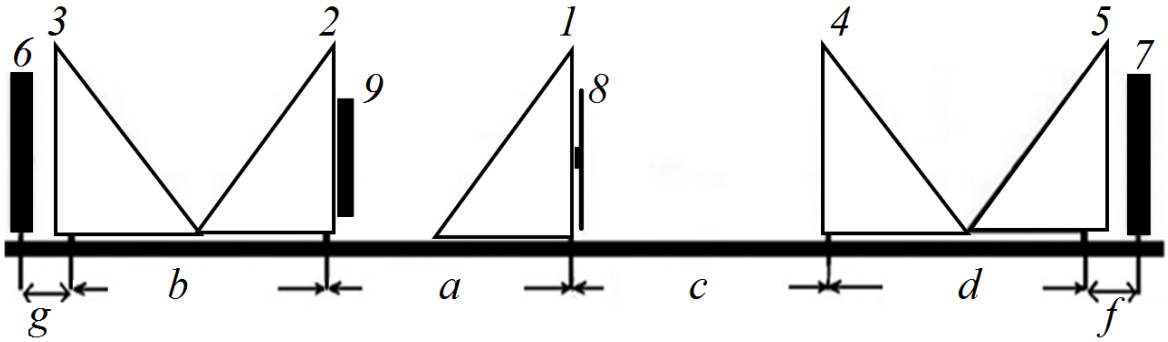

FIGURE 1. Layout of the two-armed time-of-flight LIS spectrometer. In the actual modification it includes five timing detectors, from 1 to 5, two PIN diodes (6, 7) and ^{252}Cf(sf) source (8). Additional metal foil (degrader) (9) could be placed in the detector (2). The flight-passes ($a \div d$) do not exceed 140 mm each. The distances (g) and (d) between the PIN diodes and the nearest timing detectors are near 15 mm. The spectrometer arm to the left from the start detector (1) will be called below as "arm-1" while the opposite one as "arm-2".

RESULTS

The carbon degrader, 9.6 um thick, facing the arm-1, was used in the experiment under discussion. As can be inferred from figure 2, the degrader is thick enough to cut off the low energy part of the FF heavy mass peak. The energy E_{1lin} without correction for the pulse-height defect is shown.

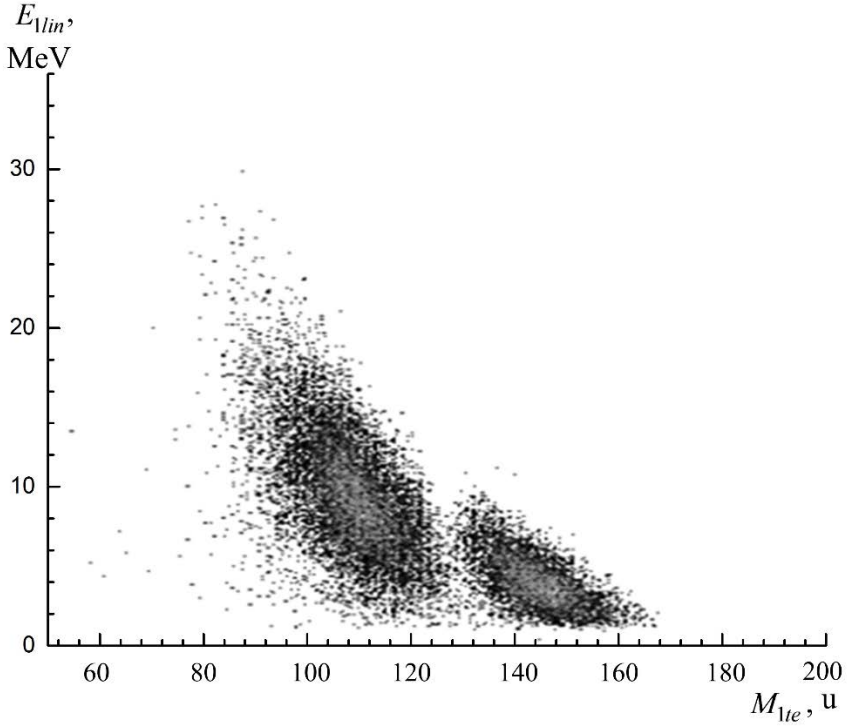

FIGURE 2. Mass-energy distribution of the fragments after passing of the carbon degrader. A low energy part of the heavy mass peak is cut off.

The FF masses before and after passing of the degrader are compared event-by-event in figure 3.

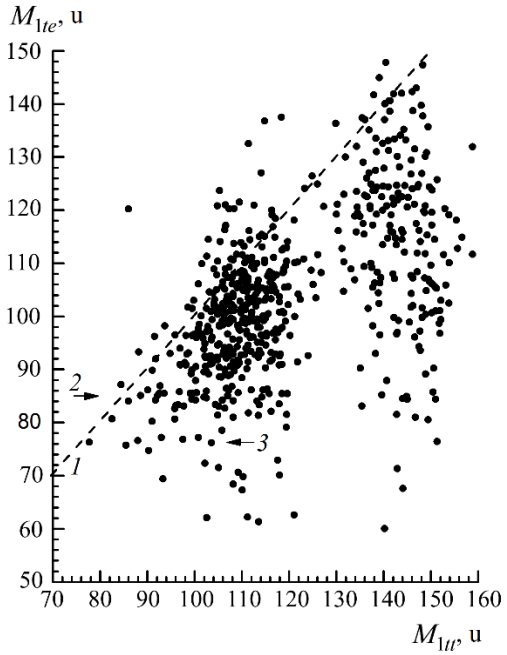

FIGURE 3. Distribution of the masses of the FF before (M_{1tt}) and after (M_{1te}) it passes the degrader. The dashed line (1) marks the points with equal masses $M_{1tt} = M_{1te}$. Specific linear structure marked by the arrows is seen in the light mass peak. The line (2) corresponds presumably to the magic isotope of ^{85}As, while line (3) to also magic isotope of ^{77}Zn. See text for details.

The linear structure, at least in the light FF mass peak, is clearly seen. More structure that is complicated is observed as well in the heavy peak with slightly large statistics (figure 4).

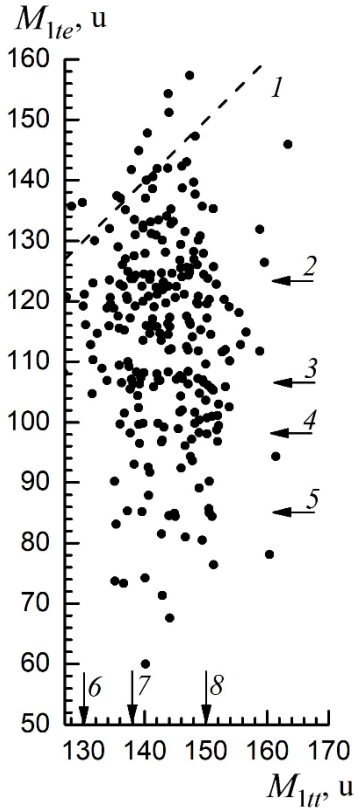

FIGURE 4. Distribution of the fragments from the heavy FF mass peak before (M_{1tt}) and after (M_{1te}) the fragment passes the degrader. The dashed line (1) marks the points with equal masses $M_{1tt} = M_{1te}$. The structure consisting of some rectangles bounded by magic isotopes is observed. The sides of the rectangles are marked by the numbered arrows and correspond presumably to the following magic isotopes: ^{121}Ag, ^{123}Cd (2), ^{108}Mo (3), ^{98}Sr (4), ^{82}Ge, ^{84}Se (5), ^{130}Sn (6), ^{138}I (7), ^{150}Ce (8). See text for details

Figure 5 shows the projection of the mass-mass distribution from figure 4 onto M_{1te} axis in order to demonstrate statistical significance of the most pronounced peaks.

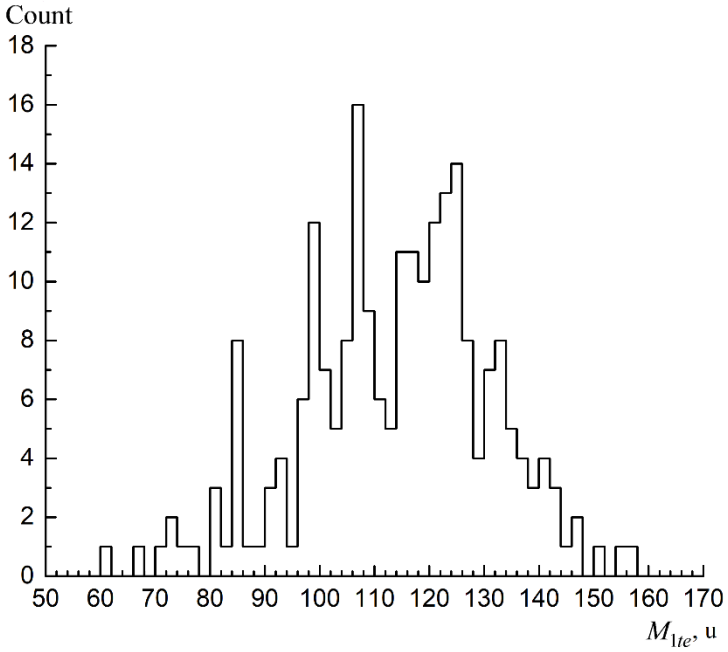

FIGURE 5. Projection of the mass-mass distribution shown in figure 4 onto M_{1te} axis. The most pronounced peaks, centered at the mass numbers $A \sim 100$ and $A \sim 108$, correspond to the lines (3, 4) in figure 4.

DISCUSSION

For the first time we have observed fragmentation of the FF from the light mass peak with the passage of the foil (figure 3). The line (2) $M_{1te} = 85$ u starts from the point $M_{1tt} = 85$ u, where $M_{1te} = M_{1tt}$, i.e. missing mass is absent in this point. The line continues up to the M_{1tt} mass partition 120/132. The sum of the facts can be treated as follows. There is the fission mode of ^{252}Cf nucleus with the prescission configuration of the fissioning system consisting of the light (^{85}As) and heavy (^{132}Sn) magic clusters connected by the neck, including the rest of the nucleons. The magic of ^{85}As is conditioned by the strongly deformed neutron shell $N \sim 85$ [4] and the heavy cluster is the double magic spherical ^{132}Sn nucleus [5]. In conventional binary fission, the ruptures occur along all the length of the neck that leads to the formation of the light FF in the mass range 85–120 u. With the passage of the foil, the light FF loses the nucleons beyond the magic core (^{85}As). The key point in the scenario is that the magic core is supposed to be already preformed in the light fragment after its forming, and the "memory" about this circumstance is conserved at least for fourteen nanoseconds (mean flight time between the Cf source and the degrader) till the FF interaction with the degrader. In other words, the light FF under discussion is likely borne in the shape isomer state with the life time at least in the nanoseconds range.

Similar scenario stands behind the line (3) in figure 3. Presumably it is a manifestation of the fission mode built on the magic ^{77}Zn and ^{148}Ce [6] as the side clusters connected by the neck. In conventional binary fission, the ruptures can occur along all of the neck. Passing the degrader, the light FF undergoes binary brake-up which results in the release of its magic core.

More complicated rectangular structures are observed in the heavy mass peak (figure 4). Let us discuss the most pronounced structure namely the rectangle bounded by the lines marked by the numbered arrows (3, 4, 7, 8). The mass correlations observed could be explained in the frame of the following scenario. At some stage of the descent from the fission barrier in the valley of the symmetric nuclear shapes [7] the chain of clusters shown in Fig. 6 is preformed with the side constituents (1, 2) to be the deformed magic nuclei of ^{98}Sr and ^{138}I

[5, 6]. The ruptures along the neck result in forming of the heavy FF with the M_{1tt} = (154÷138) u. All these fragments undergo the bake-up in the degrader showing the ^{98}Sr as the detected product. For explanation of this fact, it is reasonable to suppose that the Sr cluster is preformed in the body of the ^{138}I nucleus (figure 6). Likely, the ^{40}S and ^{98}Sr are the most preferable components for clusterization of the ^{138}I nucleus while it deforms in the process of elongation of the ^{252}Cf nucleus just before scission. The vertical line M_{1tt} = 138 u which bounds the rectangle under discussion from the left side is due to the nucleon transfer from the cluster (4) to the cluster (5) after they become free due to the brake-up of the ^{138}I nucleus in the degrader. In other words, we observe how the magic ^{98}Sr nucleus "completes" up to the next magic shell in heavier magic nuclei of ^{106}Nb and ^{108}Mo [6] (line 3 in figure 4).

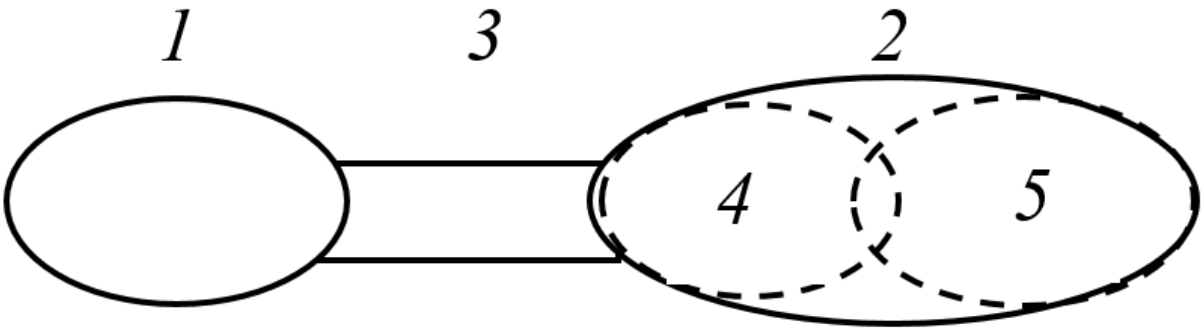

FIGURE 5. Presumable prescission configuration giving rise to the line (4) in figure 5. The constituents involved are numbered as follows: 1 – ^{98}Sr, 2 – ^{138}I, 3 – the neck corresponding to ^{16}C nucleus by the nucleon composition, 4 – ^{40}S, 5 – ^{98}Sr.

Similar process is decisive for the forming of the vertical lines M_{1tt} = (146÷154) u. These masses correspond to nuclei from ^{146}Ce to ^{154}Nd with the number of protons Z = 58–60 from the region on the map of shell corrections with a noticeable negative shell correction for the quadrupole strain parameter $\beta_2 \approx 0.4$ [6]. Isotope masses were estimated in the framework of the hypothesis of constant charge density.

Again, the ^{98}Sr cluster plays a role of the acceptor for the nucleons from the lighter clusters analogous to the ^{40}S (figure 6). The question arises why we do not observe similar vertical lines starting from all the M_{1tt} = (138÷154) u? Likely, it is important that the masses at the ends of this mass interval correspond to the magic nuclei as it was mentioned above. Immediately after its formation, the deformed heavy fragment with magic nucleon composition is already clusterized into ^{98}Sr and additional light cluster. Due to such composition, the fragment undergoes the binary brake-up in the degrader. In contrast, in the non-magical heavy fragment three clusters are preformed (figure 6), namely some part of the neck (3), cluster (4) and cluster (5). Then the ternary brake-up can occur in the degrader with the kinematics preventing further nucleon transfer between the decay partners.

Similar scenario could explain the less pronounced rectangles above and below the analyzed one. They differ by the magic clusters involved (the clusters are listed in the caption to figure 4).

CONCLUSION

The results discussed here give evidence that the FFs from conventional binary fission are born in the shape isomer states both in the fission valley of the mass-symmetric and mass-asymmetric shapes. This obstacle reflects the basic feature of the multimode nuclear fission: preformation of two magic cores in the body of the fissioning nucleus that defines its further

evolution till fission. These mode-forming cores are revealed due to the FF brake-up in the degrader. The effect has been observed for the first time.

ACKNOWLEDGMENTS

This work was supported by the research project № 18-32-00538 of the Russian Foundation for Basic Research (RFBR) and partially by the MEPhI Academic Excellence Project (Contract No. 02.a03.21.0005, 27.08.2013) of the Russian Science Foundation, as well as by the Department of Science and Technology of the Republic of South Africa (RSA).

REFERENCES

1. Yu.V. Pyatkov et al., Proceedings of the 22th International Seminar on Interaction of Neutrons with Nuclei, 2014, p. 83.
2. Yu.V. Pyatkov et al., International Symposium on Exotic Nuclei “EXON-2014”, Conference proceedings, World Scientific Publishing Co. Pte. Ltd, 2015, p. 383.
3. Yu.V. Pyatkov et al., International Symposium on Exotic Nuclei “EXON-2016”, Conference proceedings, World Scientific Publishing Co. Pte. Ltd, 2017, p. 284.
4. S.I. Mulgin et al., Nucl. Phys. A **640**, 375 (1998).
5. B.D. Wilkins et al., Phys. Rev. C **14**, 1832 (1976).
6. H. Märton, Proceedings of the “Seminar on Fission Pont D’Oye II. 1991, p. 15.
7. Yu.V. Pyatkov et al., Nucl. Phys. A**624**, 140 (1997).